Supplementary Information for:

Differential cortical microstructural maturation in the preterm human brain with diffusion kurtosis and tensor imaging

Minhui Ouyang [a,b,1], Tina Jeon [a,b,1], Aristeidis Sotiras [c], Qinmu Peng [a,c], Virendra Mishra [b,d], Cathy Halovanic [g], Min Chen [e], Lina Chalak [f], Nancy Rollins [g], Timothy Roberts [a,c], Christos Davatzikos [c], Hao Huang [a,b,c,2]

[a]Radiology Research, Children's Hospital of Philadelphia, 3401 Civic Center Boulevard, Philadelphia, PA, 19104, United States
[b]Advanced Imaging Research Center, University of Texas Southwestern Medical Center, 5323 Harry Hines Boulevard, Dallas, TX, 75390, United States
[c]Department of Radiology, Perelman School of Medicine, University of Pennsylvania, 3400 Spruce Street, Philadelphia, PA 19106, United States
[d]Lou Ruvo Center for Brain Health, Cleveland Clinic, 888 West Bonneville Avenue, Las Vegas, NV, 89106, USA
[e]Department of Mathematical Sciences, University of Texas at Dallas, 800 West Campbell Road, Richardson, TX, 75080, United States
[f]Department of Pediatrics, University of Texas Southwestern Medical Center, 5323 Harry Hines Boulevard, Dallas, TX, 75390, United States
[g]Department of Radiology, University of Texas Southwestern Medical Center, 5323 Harry Hines Boulevard, Dallas, TX, 75390, United States

[1] M.O. and T.J. contributed equally to this work.

[2]Corresponding Author:
Hao Huang, PhD
Email: huangh6@email.chop.edu

This PDF file includes:

Supplementary text
Figs. S1 to S4
Tables S1 to S4
Legends for movies S1 to S7
References for SI reference citations

Other supplementary materials for this manuscript include the following:

Movies S1 to S7

Supplemental Information

SI Materials and Methods

Participants. Informed parental consents were obtained from the subject's parent. All recruited infants were not clinically indicated. They were recruited completely for research purpose which was studying normal prenatal and perinatal brain development. All infants were selected after rigorous screening procedures conducted by an experienced neonatologist (LC) and an experienced pediatric radiologist (NR), based on subjects' ultrasound, clinical MRI and subjects' and mothers' medical record. The exclusion criteria included evidence of bleeding or intracranial abnormality by serial sonography; the mother's excessive drug or alcohol abuse during pregnancy; periventricular leukomalacia; hypoxic–ischemic encephalopathy; Grade III–IV intraventricular hemorrhage; body or heart malformations; chromosomal abnormalities, lung disease or bronchopulmonary dysplasia; necrotizing enterocolitis requiring intestinal resection or complex feeding/nutritional disorders; defects or anomalies of the brain; brain tissue dysplasia or hypoplasia; abnormal meninges; alterations in the pial or ventricular surface; or white matter (WM) lesions. Out of 107 neonates who were consented, diffusion MRI (dMRI) was acquired from 89 neonates. Table S1 lists demographics of the 76 normal neonates (47 M/ 29 F; post-menstrual ages: 31.5 to 41.7 postmenstrual weeks (PMW)) whose dMRI scans were included in this study. DMRI datasets of 13 subjects were not included in the study due to significant motion artifacts.

MRI data acquisition. A single-shot echo-planar imaging (EPI) sequence with Sensitivity Encoding parallel imaging (SENSE factor = 2.5) was used for dMRI. The multi-shell dMRI parameters were: echo time (TE) = 78ms, repetition time (TR) = 6850ms, field of view = 168/168/96mm, imaging matrix = 112x112mm, axial slice thickness = 1.6mm without gap, 30 gradient directions, b values = 0, 1000, and 1600 sec/mm^2. To increase signal to noise ratio (SNR), two repetitions were performed for both b = 1000 sec/mm^2 and b = 1600 sec/mm^2, resulting in a total scan time of 18 minutes for dMRI acquisition with both b=1000 and 1600 sec/mm^2 and a total scan time of 9 minutes for dMRI acquisition with b=1000 sec/mm^2 only. Of the 76 subjects whose dMRI are included in this study, 26 (19 M/ 7 F; 33.4 to 40.7PMW) were scanned with two b-values (Table S1).

Measurement of DKI and DTI metrics on the parcellated cortical skeleton. The cortical skeleton was created from averaged fractional anisotropy (FA) maps or cortical segmentation maps in three age-specific templates at 33, 36 and 39PMW due to dramatic anatomical changes of the neonate brain from 31 to 42PMW (1). Each subject brain was categorized into 3 age groups at 33, 36 and 39PMW based on the age and registered to the corresponding template at 33, 36 or 39PMW using the registration protocol (2). After resampled to isotropic resolution, diffusion weighted images (DWIs) of all subjects were first linearly registered to a single subject template at 33, 36 or 39 PMW using rigid and affine transformation in *Diffeomap* (http://www.mristudio.org) with the contrasts of skull-stripped b0 driving the registration. The DWIs of all subjects were then nonlinearly registered to the single subject template at 33, 36 or 39PMW using *LDDMM* (Large Deformation Diffeomorphic Metric Mapping) in *Diffeomap* with the dual-contrasts of FA and b0 images driving the registration. Cortical skeleton of the 33PMW or 36PMW brain was extracted from the averaged cortical FA map with skeletonization function in *TBSS* of *FSL* (http://fsl.fmrib.ox.ac.uk/fsl/fslwiki/TBSS). Due to low cortical FA in the 39PMW brains, cortical skeleton of the 39PMW brain was obtained with averaged cortical segmentation map at 39PMW using the method in the literature (3). Specifically, cortical segmentation of each 39PMW brain was obtained by applying FAST (FMRIB's Automated Segmentation Tool) to the MD map. The segmented cortical plate was transformed to the template space of the 39PMW brain using the transformation described in *SI Materials and Methods*. Skeletonization function was applied to the averaged cortical segmentation map to obtain the cortical skeleton at 39PMW. Based on the age of the subject, the cortical skeleton in the 33, 36 or 39PMW template space was then inversely

transferred to each subject's native space (Fig. S1A), to which the cortical gyral labels of the JHU neonate atlas (2) were also mapped to parcellate the cortex (Fig. S1B). The parcellated cortical skeleton was obtained (Fig. S1C) by directly overlapping the cortical skeleton in Fig. S1A with the JHU neonate atlas labels in Fig. S1B. Fig. S1D shows the cortical tissue segmentation based on MD map in the native space. Irregularly small yet significant offsets between the cortical skeleton and subject's cerebral cortex were widespread, due to imperfect inter-subject registration from transforming cortical skeletons to individual brains. At a given cortical skeleton voxel, the offset between the cortical skeleton and core of the cerebral cortex was corrected by projecting the DTI and DKI measurements from surrounding voxels with the highest gray matter tissue probability (yellow in Fig. S1E) to the corresponding cortical skeleton voxels (cyan line in Fig. S1E). In this way, the cortical DKI- and DTI-derived parameters were measured at the core cortical regions. DKI- or DTI-derived parameters at each cortical gyrus was obtained by averaging the measurements on the cortical skeleton voxels with the same cortical gyral label. All DKI- or DTI-derived maps at an individual PMW were displayed on a partially inflated surface on a 35PMW brain. Before registration from the native space to the 35PMW brain template, DKI- or DTI-derived parameter measurements on the cortical skeleton voxels were assigned to all voxels in a dilated cortical ribbon in the native space using fast marching (4). After registration, the cortical DKI- or DTI-derived measurements of the same PMW were then averaged in the 35PMW brain template. In this way, the errors of projecting the cortical skeleton measurements to the 35PMW brain surface due to imperfect inter-subject registration were minimized.

Clustering analyses. Non-negative Matrix Factorization (NMF) was used to approximate the data through a set of new variables $\boldsymbol{W}$ that were combined according to the set of coefficients given by $\boldsymbol{C}$. The new variables, termed hereafter components, were constructed as a linear, non-negative combination of the original variables. NMF aggregated variance in the components by positively weighting original variables (i.e., cortical microstructural measurements) that tend to co-vary (5). Thus, NMF isolated patterns of regional co-variation of time courses of cortical mean kurtosis (MK) and FA at cortical skeleton voxels. The integrity of the i^{th} cluster in the j^{th} sample is summarized by the non-negative scalar value c_{ij}. The components can be represented as soft cluster assignment maps, where the distribution of the coefficient values of cortical MK or FA exhibiting similar statistical properties peaks for the same component. In this study, cluster number of 4 were selected for categorizing the time courses of both cortical MK and FA with following two reasons. First, coarse cluster model was used to delineate cortical microstructure pattern in preterm infants previously (3). Second, the complementary properties of FA and MK may be better reflected with relatively coarse clusters rather than fine ones as the fine clusters based on brain gyral or sulcal geometry or functional specialization already exist.

White matter tractography using cortical clusters as the seed. Diffusion-tensor-imaging-based (DTI-based) tractography was used to trace the white matter (WM) fibers of the 26 subjects whose multi-shell diffusion MRI datasets were acquired. Tracing was initialized from the four largest cortical clusters obtained from the clustering analysis of cortical MK (Figure 2B). The largest cluster from each of four clustering results was extracted and then dilated by 2 mm using custom software in IDL (Interactive Data Language 8.2.3, http://www.exelisvis.com) to penetrate the gray-white matter mixed area and reach the deep WM to initiate fiber tracking (6). Fiber tracing was conducted using DTI Studio (http://www.mristudio.org). The FA value of the WM tract traced from each of the four largest cortical clusters was calculated after applying a FA threshold of 0.15 to remove the non-WM (such as cerebrospinal fluid) voxels.

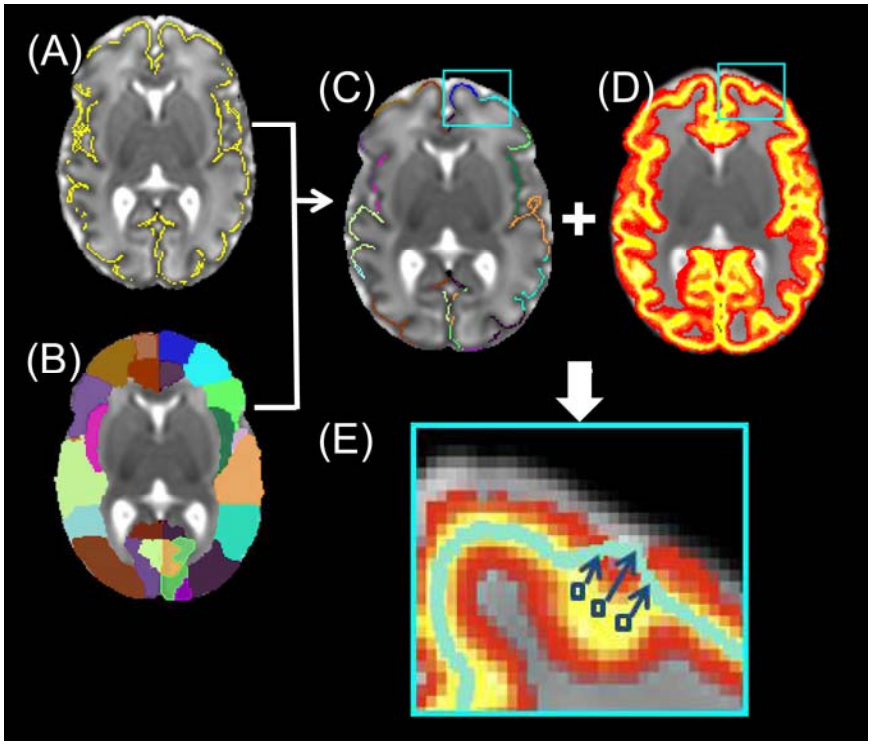

Fig. S1: The workflow to parcellate and measure the cortical DTI and DKI metrics at the neonate cortical skeleton. (A) Yellow cortical skeleton overlaid on the mean diffusivity map of a 33 PMW neonate brain; (B) the gyral labels with different colors denoting different gyri labels transferred from the JHU neonate atlas; (C) the labeled cortical skeleton; (D) the cortical tissue probability map; (E) Enlarged map showing measurement of MK or FA at the cortical skeleton (cyan line) projected from nearby voxels with maximum gray matter probability (dark blue boxes).

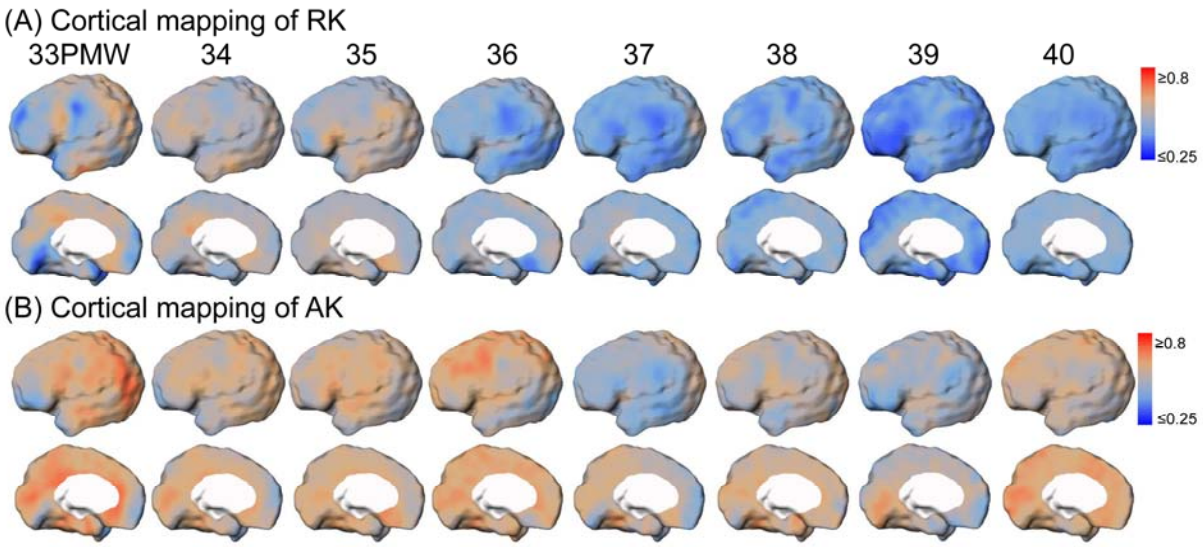

Fig. S2: Spatiotemporal changes of DKI-derived radial (RK) (A) and axial (AK) (B) kurtosis measurement maps of preterm brain cerebral cortex from 33 to 40PMW.

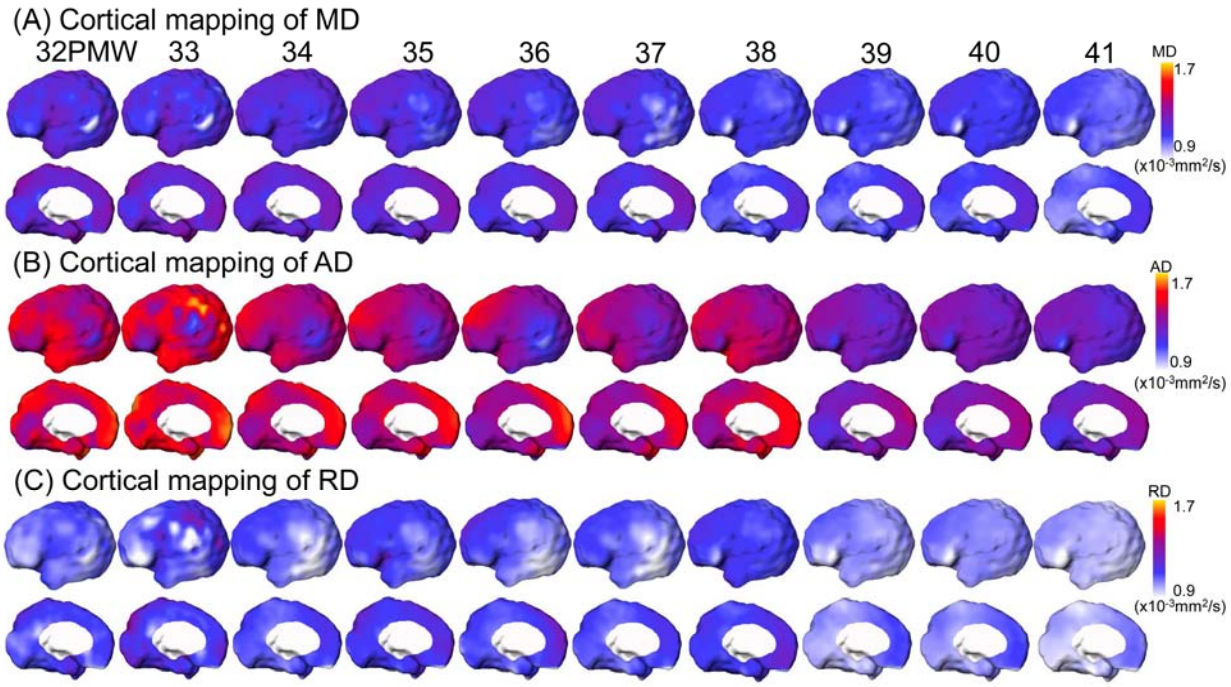

Fig. S3: Spatiotemporal changes of DTI-derived mean (MD) (A), axial (AD) (B) and radial (RD) (C) diffusivity measurement maps of preterm brains cerebral cortex from 32 to 41 PMW.

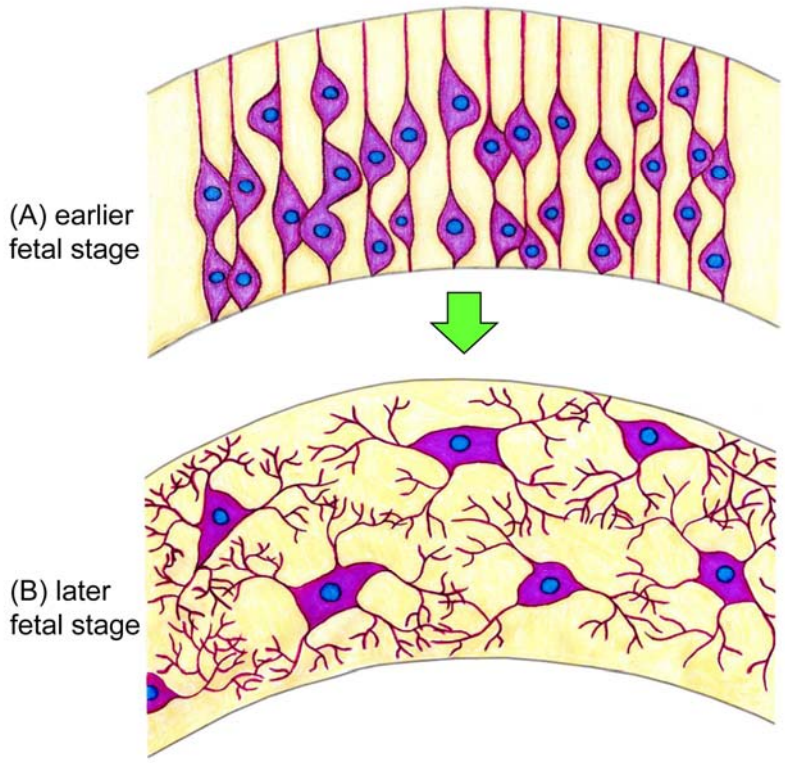

Fig. S4: Schematic depiction of dendritic arborization and cell deaths from 30PMW to 40PMW that may underlie cortical MK and FA changes. Panel (A) shows the cerebral cortical organization including the immature neurons and radial glia scaffold perpendicular to the cortical surface during earlier fetal stage. Panel (B) shows that the cell density has decreased through apoptosis concurrently with the increases in cortical neuropil and basal dendrites during later fetal stage. These processes jointly result in overall reduction of the diffusion barriers associated with a decrease in cortical MK and overall reduction of the organized cytoarchitecture associated with a decrease in cortical FA.

Table S1: Demographics of participating subjects who were scanned with diffusion kurtosis imaging (DKI) and diffusion tensor imaging (DTI). [a]C for C-section and V for vaginal birth; [b] B for breast-feeding and F for formula.

Group		Number of Infants	Age range (wks)	Age mean (wks)	Weight range (kgs)	Weight mean (kgs)	Male n(%)	White n(%)	Mode of delivery [a]	Feeding practice [b]	Antibiotic exposure during pregnancy
DKI	At birth	26	28.3-40.7	34.3	1.1-3.9	2.1	19 (73)	21 (81)	C:13; V:13	B: 26; F: 0	Yes
	At scan		33.4-40.7	36.8	1.4-3.9	2.4					
DTI	At birth	76	26.0-41.4	33.9	0.8-4.0	2.1	47 (62)	56 (73)	C: 25; V: 51	B: 76; F: 0	Yes
	At scan		31.9-41.7	37.1	1.4-3.9	2.5					

Table S2: Pearson correlation r values, p values, and slopes of the cortical gyri for mean kurtosis (MK) decease, fractional anisotropy (FA) decrease with age<36.4wks and FA flat portion with age>36.4 wks. P values less than 0.05 are highlighted in bold. FDR-corrected p values less than 0.05 are highlighted in bold and with underline. wk: week.

		MK			FA (age < 36.4 wks)			FA (age > 36.4 wks)		
Gyri	Left/ Right	r	p	slope (1/wk)	r	p	slope (1/wk)	r	p	slope (1/wk)
Superior frontal gyrus	Left	-0.51	**0.0061**	-0.0253	-0.48	**1.1E-05**	-0.0075	0.12	0.2973	0.0011
Superior frontal gyrus	Right	-0.40	**0.0386**	-0.0197	-0.54	**4.2E-07**	-0.0090	0.14	0.2250	0.0013
Middle frontal gyrus	Left	-0.41	**0.0345**	-0.0210	-0.74	**2.9E-14**	-0.0159	-0.07	0.5758	-0.0006
Middle frontal gyrus	Right	-0.54	**0.0036**	-0.0246	-0.68	**1.1E-11**	-0.0129	0.11	0.3379	-0.0006
Inferior frontal gyrus	Left	-0.38	**0.0466**	-0.0161	-0.65	**1.4E-10**	-0.0106	-0.03	0.8259	-0.0002
Inferior frontal gyrus	Right	-0.65	**2.2E-04**	-0.0278	-0.65	**1.4E-10**	-0.0101	0.20	0.0796	0.0014
Medial fronto-orbital gyrus	Left	-0.59	**0.0011**	-0.0254	-0.49	**5.5E-06**	-0.0089	0.09	0.4189	0.0012
Medial fronto-orbital gyrus	Right	-0.49	**0.0086**	-0.0212	-0.48	**1.2E-05**	-0.0099	-0.11	0.3419	-0.0013
Lateral fronto-orbital gyrus	Left	-0.51	**0.0063**	-0.0217	-0.39	**5.3E-04**	-0.0065	0.19	0.1019	0.0021
Lateral fronto-orbital gyrus	Right	-0.54	**0.0038**	-0.0218	-0.40	**4.0E-04**	-0.0062	0.29	**0.0124**	0.0029
Gyrus rectus	Left	-0.74	**8.9E-06**	-0.0346	-0.58	**2.7E-08**	-0.0124	-0.17	0.1412	-0.0124
Gyrus rectus	Right	-0.70	**4.8E-05**	-0.0302	-0.59	**2.0E-08**	-0.0104	-0.18	0.1189	-0.0016
Precentral gyrus	Left	-0.44	**0.0211**	-0.0204	-0.16	0.1555	-0.0023	0.41	**2.8E-04**	0.0026
Precentral gyrus	Right	-0.50	**0.0076**	-0.0246	-0.19	0.0981	-0.0021	0.34	**0.0027**	0.0035
Postcentral gyrus	Left	-0.42	**0.0280**	-0.0196	-0.18	0.1252	-0.0022	0.43	**8.7E-05**	0.0030
Postcentral gyrus	Right	-0.62	**5.4E-04**	-0.0302	-0.28	**0.0133**	-0.0039	0.34	**0.0027**	-0.0025
Superior parietal lobule	Left	-0.48	**0.0118**	-0.0277	-0.46	**3.1E-05**	-0.0072	0.11	0.3417	0.0010
Superior parietal lobule	Right	-0.49	**0.0088**	-0.0303	-0.39	**4.6E-04**	-0.0059	0.25	**0.0290**	0.0010
Precuneus	Left	-0.52	**0.0055**	-0.0276	-0.54	**4.8E-07**	-0.0086	0.23	**0.0287**	-0.0013
Precuneus	Right	-0.52	**0.0050**	-0.0298	-0.59	**2.5E-08**	-0.0104	0.18	0.1263	-0.0104
Supramarginal gyrus	Left	-0.45	**0.0181**	-0.0273	-0.46	**2.3E-05**	-0.0078	0.40	0.3458	0.0008
Supramarginal gyrus	Right	-0.63	**3.4E-04**	-0.0361	-0.56	**1.2E-07**	-0.0098	0.27	0.5461	-0.0006
Angular gyrus	Left	-0.56	**0.0023**	-0.0335	-0.59	**1.5E-08**	-0.0100	0.40	0.9172	-0.0100
Angular gyrus	Right	-0.55	**0.0028**	-0.0361	-0.62	**1.5E-09**	-0.0100	0.27	0.1774	-0.0013
Superior temporal gyrus	Left	-0.59	**0.0011**	-0.0231	-0.49	**6.2E-06**	-0.0083	0.40	0.4499	0.0006
Superior temporal gyrus	Right	-0.68	**9.2E-05**	-0.0252	-0.56	**1.1E-07**	-0.0094	0.27	0.0720	0.0014
Middle temporal gyrus	Left	-0.61	**7.4E-04**	-0.0234	-0.66	**7.4E-11**	-0.0121	0.40	0.2810	-0.0010
Middle temporal gyrus	Right	-0.80	**4.4E-07**	-0.0365	-0.57	**7.3E-08**	-0.0114	0.27	**0.0293**	-0.0022
Inferior temporal gyrus	Left	-0.61	**6.7E-04**	-0.0216	-0.53	**1.0E-06**	-0.0109	0.40	**0.0063**	-0.0022
Inferior temporal gyrus	Right	-0.78	**1.3E-06**	-0.0336	-0.55	**2.5E-07**	-0.0106	0.27	**0.0323**	-0.0022
Fusiform gyrus	Left	-0.55	**0.0030**	-0.0167	-0.44	**7.9E-05**	-0.0074	0.40	**3.8E-04**	0.0039
Fusiform gyrus	Right	-0.64	**2.8E-04**	-0.0251	-0.42	**1.8E-04**	-0.0073	0.27	**0.0193**	-0.0010
Cingular gyrus	Left	-0.67	**1.3E-04**	-0.0277	-0.41	**2.5E-04**	-0.0054	0.55	**2.9E-07**	0.0055
Cingular gyrus	Right	-0.58	**0.0014**	-0.0242	-0.40	**3.3E-04**	-0.0049	0.46	**2.3E-05**	0.0041
Superior occipital gyrus	Left	-0.53	**0.0045**	-0.0322	-0.53	**7.2E-07**	-0.0109	0.15	0.1943	0.0013
Superior occipital gyrus	Right	-0.48	**0.0109**	-0.0305	-0.64	**5.2E-10**	-0.0151	0.27	**0.0193**	0.0027
Middle occipital gyrus	Left	-0.55	**0.0026**	-0.0350	-0.58	**5.0E-08**	-0.0117	0.02	0.8743	0.0001
Middle occipital gyrus	Right	-0.53	**0.0045**	-0.0362	-0.63	**8.1E-10**	-0.0124	-0.06	0.6140	-0.0005
Inferior occipital gyrus	Left	-0.54	**0.0033**	-0.0304	-0.55	**1.9E-07**	-0.0113	0.15	0.1867	0.0014
Inferior occipital gyrus	Right	-0.56	**0.0020**	-0.0362	-0.70	**1.4E-12**	-0.0137	0.15	0.1827	0.0014
Cuneus	Left	-0.58	**0.0015**	-0.0301	-0.63	**8.6E-10**	-0.0114	0.18	0.1259	0.0015

Cuneus	Right	-0.58	**0.0015**	-0.0335	-0.67	**3.3E-11**	-0.0129	0.31	**0.0068**	0.0031
Lyngual gyrus	Left	-0.58	**0.0014**	-0.0229	-0.58	**5.1E-08**	-0.0101	0.47	**1.6E-05**	0.0046
Lyngual gyrus	Right	-0.47	**0.0124**	-0.0192	-0.60	**1.1E-08**	-0.0100	0.33	**0.0034**	0.0033
Insular cortex	Left	-0.58	**0.0016**	-0.0210	-0.38	**6.8E-04**	-0.0050	0.22	0.0574	0.0016
Insular cortex	Right	-0.69	**5.3E-05**	-0.0297	-0.55	**2.4E-07**	-0.0096	0.07	0.5329	0.0007

Table S3: Partial correlation between the cortical MK and FA measurements of all cortical gyri after controlling for age. Partial correlation r values and FDR-corrected p values are listed.

Gyri	Left Hemisphere		Right Hemisphere	
	r	FDR-corrected p	r	FDR-corrected p
Superior frontal gyrus	0.18	0.1856	0.07	0.1914
Middle frontal gyrus	0.26	0.3809	0.07	0.1863
Inferior frontal gyrus	0.19	0.1964	-0.12	0.1860
Medial fronto-orbital gyrus	-0.09	0.1963	-0.03	0.1818
Lateral fronto-orbital gyrus	-0.08	0.1962	-0.16	0.1919
Gyrus rectus	0.14	0.1946	0.03	0.1801
Precentral gyrus	0.06	0.1860	0.16	0.2001
Postcentral gyrus	-0.01	0.1853	0.11	0.1784
Superior parietal lobule	0.08	0.1883	0.24	0.2741
Precuneus	0.23	0.2221	0.33	0.2354
Supramarginal gyrus	-0.15	0.1925	-0.03	0.1804
Angular gyrus	0.05	0.1821	-0.05	0.1854
Superior temporal gyrus	0.08	0.1924	0.23	0.2575
Middle temporal gyrus	-0.02	0.1799	0.16	0.1887
Inferior temporal gyrus	0.04	0.1781	0.06	0.1896
Fusiform gyrus	0.13	0.1790	0.25	0.2954
Cingular gyrus	0.19	0.1922	0.13	0.1837
Superior occipital gyrus	0.22	0.1933	0.22	0.2048
Middle occipital gyrus	0.12	0.1822	0.05	0.1867
Inferior occipital gyrus	0.13	0.1904	0.22	0.1833
Cuneus	0.20	0.1908	0.39	0.2343
Lyngual gyrus	0.25	0.3212	0.35	0.2542
Insular cortex	0.23	0.2319	0.48	0.1430

Movie Legends

Movie S1: 4D spatiotemporal dynamics of cortical MK measurement during 33-40PMW.

Movie S2: 4D spatiotemporal dynamics of cortical RK measurement during 33-40PMW.

Movie S3: 4D spatiotemporal dynamics of cortical AK measurement during 33-40PMW.

Movie S4: 4D spatiotemporal dynamics of cortical FA measurement during 32-41PMW.

Movie S5: 4D spatiotemporal dynamics of cortical MD measurement during 32-41PMW.

Movie S6: 4D spatiotemporal dynamics of cortical RD measurement during 32-41PMW.

Movie S7: 4D spatiotemporal dynamics of cortical AD measurement during 32-41PMW.

References

1. Feng L, et al. (2018) Age-specific gray and white matter DTI atlas for human brain at 33, 36 and 39 postmenstrual weeks. *Neuroimage* (in press) https://doi.org/10.1016/j.neuroimage.2018.06.069
2. Oishi K, et al. (2011) Multi-contrast human neonatal brain atlas: application to normal neonate development analysis. *Neuroimage* 56(1):8-20.
3. Ball G, et al. (2013) Development of cortical microstructure in the preterm human brain. *Proc Natl Acad Sci USA* 110(23):9541-9546.
4. Jeon T, et al. (2012) Regional changes of cortical mean diffusivities with aging after correction of partial volume effects. *Neuroimage* 62(3):1705-1716
5. Sotiras A, et al. (2017) Patterns of coordinated cortical remodeling during adolescence and their associations with functional specialization and evolutionary expansion. *Proc Natl Acad Sci USA* 114(13):3527-3532
6. Jeon T, Mishra V, Ouyang M, Chen M, Huang H (2015) Synchronous changes of cortical thickness and corresponding white matter microstructure during brain development accessed by diffusion MRI tractography from parcellated cortex. *Front Neuroanat* 9:158.